Quantum cascade transmitters for ultra-sensitive chemical agent and explosives detection

John F. Schultz*[a], Matthew S. Taubman[a], Warren W. Harper[a], Richard M. Williams[a], Tanya L. Myers[a], Bret D. Cannon[a], David M. Sheen[a], Norman C. Anheier[a], Paul J. Allen[a], S.K. Sundaram[a], Bradley R. Johnson[a], Pamela M. Aker[a], Ming C. Wu[b], Erwin K. Lau[b]
[a]Pacific Northwest National Laboratory (PNNL); [b]Dept. of Electrical Engineering, University of California Los Angeles (UCLA)

ABSTRACT

The small size, high power, promise of access to any wavelength between 3.5 and 16 microns, substantial tuning range about a chosen center wavelength, and general robustness of quantum cascade (QC) lasers provide opportunities for new approaches to ultra-sensitive chemical detection and other applications in the mid-wave infrared. PNNL is developing novel remote and sampling chemical sensing systems based on QC lasers, using QC lasers loaned by Lucent Technologies. In recent months laboratory cavity-enhanced sensing experiments have achieved absorption sensitivities of 8.5 x 10^{-11} cm^{-1} $Hz^{-1/2}$, and the PNNL team has begun monostatic and bi-static frequency modulated, differential absorption lidar (FM DIAL) experiments at ranges of up to 2.5 kilometers. In related work, PNNL and UCLA are developing miniature QC laser transmitters with the multiplexed tunable wavelengths, frequency and amplitude stability, modulation characteristics, and power levels needed for chemical sensing and other applications. Current miniaturization concepts envision coupling QC oscillators, QC amplifiers, frequency references, and detectors with miniature waveguides and waveguide-based modulators, isolators, and other devices formed from chalcogenide or other types of glass. Significant progress has been made on QC laser stabilization and amplification, and on development and characterization of high-purity chalcogenide glasses, waveguide writing techniques, and waveguide metrology.

Keywords: Quantum cascade lasers, chemical sensing, frequency modulation lidar, cavity-enhanced sensor, integrated optics

1. INTRODUCTION

An important class of spectroscopic chemical sensors determines the presence of one or more molecular species of interest (analytes) in a sample volume of air by comparing the spectral dependence of light absorption in multiple air samples. The spectra of air samples may be measured remotely with lidars or passive spectrometers, or in-situ with instruments that draw air samples into special chambers for interrogation. To make the comparison, the spectra of a library of analytes and interferents are fit to the measured spectrum of each sample to determine the best-fitting combination of analyte concentrations. A sample is determined to contain an above-ambient concentration of a given analyte when the fit yields a concentration that is statistically greater than ambient. For a given analyte, then, the practical range, sensitivity (minimum detectable analyte burden), and selectivity (susceptibility to interferents) of a sensor are determined by the extent to which spectral differences due to the analyte concentration can be separated from spectral differences due to many forms of instrument noise, and due to natural fluctuations in a wide variety of ambient conditions. Examples of instrument noise effects are laser speckle; fluctuations in laser power, wavelength, or phase; signal shot noise; calibration errors; and the many components of photo-detector and amplifier noise. Examples of fluctuations in ambient conditions are variations in atmospheric chemical content, chemical distribution, or temperature, and variations in ground surface materials, geometry, or temperatures. Selection of analyte spectral features with the best combination of absorption strength and spectral uniqueness is therefore of key importance to optimizing sensors.

*john.schultz@pnl.gov; phone 509-375-6830; fax 509-372-4583; Pacific Northwest National Laboratory, PO Box 999, Richland, WA 99352

Quantum Sensing: Evolution and Revolution from Past to Future, Manijeh Razeghi, Gail J. Brown, Editors, Proceedings of SPIE Vol. 4999 (2003) © 2003 SPIE · 0277-786X/03/$15.00

In general, the strongest and most distinctive features of molecular spectra are transitions between rotational and vibrational states with differences in energy that correspond to infrared wavelengths between 3 and 25 microns. The spectra of most ordinary atmospheric constituents are relatively free of absorption features in two bands lying from 3 to 5 microns (mid-wave infrared - MWIR), and from 8 to 13 microns (long-wave infrared - LWIR). Interference with the atmosphere is therefore minimized in these bands, which makes them attractive for chemical sensing. At atmospheric sample pressures of interest for remote sensing, the strongest, most distinctive spectral features are "Q-branch" absorption features resulting from multiple $\Delta J = 0$ transitions with the same energy. Even at atmospheric pressure, these transitions can be a narrow as $0.1 cm^{-1}$. Most Q-branch absorptions are found in the LWIR window. In addition, the derivatives of molecular spectra often contain much narrower, more distinctive features than the spectra themselves, which opens another avenue to improving the performance of laser-based chemical sensors. Figure 1.1 compares the direct absorption spectra of four chemicals[1] and their composite with their derivatives and the derivative of the composite to illustrate these improvements in spectral uniqueness.

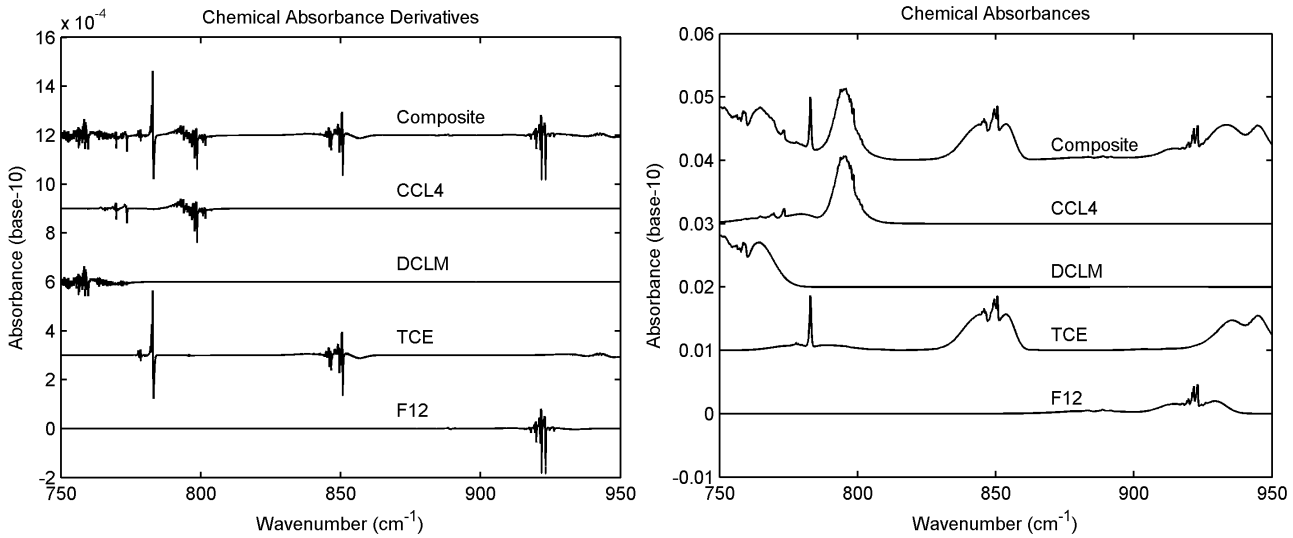

Figure 1.1: Spectra of four chemical vapors

For applications where it is possible to draw air samples into a special chamber for analysis, samples can be interrogated in optical cavities to eliminate some of the sources of noise due to fluctuations in ambient conditions. Optical cavities also increase the path-length of laser light through the sample, with proportional increases in signal to noise ratios. Sample interrogation within a chamber can be conducted at reduced pressure, which dramatically reduces interference between molecular spectra by eliminating pressure broadening. This occurs without loss of peak absorption strength, and allows use of spectral features that are even narrower than the limits imposed by Doppler broadening[2].

To date, the wavelength tuning and power achievable with lasers capable of operating in the infrared atmospheric windows have been inadequate to permit exploitation of most Q-branch spectral features, except at coincidental overlaps between Q branch features and CO_2 or other gas laser lines. Inadequate laser stability, tuning, and modulation characteristics have also impeded utilization of frequency modulation techniques sensitive to narrow features, or exploitation of the greater spectral uniqueness available at reduced pressures. Quantum cascade lasers (QCLs) or inter-band cascade lasers (ICLs) can be designed to operate at any center wavelength in these windows, however, and are continuously tunable through ranges of a few inverse centimeters about their center wavelengths[3,4]. In addition, they appear capable of producing up to 1 watt of continuous-wave (CW) optical power per laser, have shown superb stability and modulation characteristics, have cross-sectional dimensions of a few microns, and are only a few millimeters in length. Steady improvements in room temperature operation have been made[5]. The demonstrated and potential capabilities of QCLs and ICLs promise new classes of ultra-sensitive, ultra-selective sampling and short-range remote chemical sensors for a wide variety of national security and civil applications. The small sizes of QCLs and ICLs will also enable compact laser-based sensors. PNNL is therefore exploring frequency-modulated differential absorption lidar

(FM DIAL) for short-range remote chemical sensing, and a variety of cavity-enhanced sensors (CES) for in-situ chemical sensing. This research and recent progress are summarized in Section 2.

As implied in the preceding paragraphs, FM DIAL and novel CES techniques place demanding requirements on laser tuning ranges and precision, and on laser power, stability, modulation characteristics, and wavelength multiplexing. PNNL and UCLA are therefore developing QCL transmitter modules that incorporate multiple QCL devices and many other MWIR optical components to meet these requirements. Due to the small end-facet dimensions of QCLs and ICLs, infrared laser beams emerge from them with a large divergence, which complicates use of conventional free space optics for coupling to other components of transmitter modules. In addition, conventional infrared optical components such as isolators, polarizers, beam-splitters, wavelength combining and multiplexing apparatus, and Fabry-Perot optical cavities do not scale to the sizes needed to miniaturize QCL transmitter modules, particularly in the LWIR. PNNL is therefore developing LWIR waveguides and waveguide-based optical components to establish the basis for miniaturizing QCL transmitter modules through use of miniature LWIR photonic devices. The module development research is described in Section 3, and the LWIR photonics research is summarized in Section 4.

2. ADVANCED CHEMICAL SENSOR APPLICATIONS AND RECENT RESEARCH

2.1 Frequency-modulated differential absorption lidar (FM-DIAL)

As described in much greater detail by Silver[6], the time dependence of a frequency-modulated laser beam's electric field, E(t), can be described as a fundamental at frequency ω_0, plus a series of terms at the fundamental shifted by harmonics of the modulation frequency ω_m:

$$E(t) = E_0\left[1 + M\sin\left(\omega_m t + \psi\right)\right]\exp(i\omega_0 t)\left[\sum_{n=-\infty}^{\infty} J_n(\beta)\exp(in\omega_m t)\right] \quad 2.1$$

In Eq.2.1 M is the amplitude modulation coefficient, β is the phase modulation index, and J_n are Bessel functions. A photo-detector responds to the square of the magnitude of the electric field, so modulated light has potential to generate beat signals at all harmonics of the modulation frequency. If a photo-detector is illuminated with a purely frequency-modulated laser (M=0), it produces only a DC signal because the beat frequencies between all terms in Eq.2.1 cancel. This is true only as long as nothing has been done to change the relative amplitudes or phases of any terms in Eq.2.1. If the relative amplitudes of the terms in Eq.2.1 are changed by a molecular absorption prior to illuminating the detector, the beats no longer cancel, and the photo-detector sees harmonics of the modulation frequency ω_m. In the limit that the modulation frequency and the product of the modulation frequency and the phase modulation index are both much less than the width of the absorption feature, the signal at the nth harmonic of the modulation frequency is proportional to the nth derivative of the absorption spectrum with respect to frequency. With a phase modulation index adjusted for optimum signal size, the signals are no longer proportional to derivatives, but they do retain the important features of derivative spectra as long as the modulation frequency is still small. These features are enhancement of sharp spectral features, odd harmonics having dispersion shapes, and even harmonics having extrema at the absorption maxima. Because these qualitative features are retained, and improve the uniqueness of molecular spectra for purposes of chemical identification, we will continue to call the spectra of the harmonic signals derivative spectra. Continuous segments of derivative spectra can be mapped by simultaneously tuning the fundamental laser frequency ω_0 as the laser is frequency modulated at ω_m. Because the signals occur at precise frequencies chosen by the experimenter, it is possible to use narrow-band detectors and amplifiers optimized for those frequencies, and to filter many types of detector, amplifier, and background noise very effectively. FM spectroscopy is therefore a good technique for sensing the derivatives of molecular spectra - thus taking advantage of their greater uniqueness - given laser sources with the right tuning, stability, modulation, and power characteristics.

To assess the potential of FM spectroscopy for practical applications, PNNL has built a fieldable FM lidar based on QCLs[7], and is using it to explore the phenomenology and performance of FM DIAL systems in field environments. Photographs of the lidar in its cart and trailer mounted configurations are presented in Figure 2.1. Key specifications for the FM lidar are listed in Table 2.1.

Important characteristics of the FM lidar and its components have been carefully measured, and a variety of preliminary monostatic, linear bistatic, and closed-loop perimeter field experiments have been conducted. Monostatic FM DIAL field experiments were conducted at ranges up to 200 meters, and bistatic experiments incorporating a retro-reflector were conducted at round-trip ranges of up to 5 kilometers.

The preliminary monostatic experiments were conducted with a relatively low power QCL lasing at 8.2 microns, a beam transmitter that was not well matched to the receiver field of view, and without any spectral filtering. Nevertheless, at a range of 40 meters, noise-equivalent absorption sensitivities (NEAS) of 4×10^{-4} were achieved by averaging 8 seconds of data. A 14-inch x 14-inch foam target was used for a background. Analysis of the data indicates that range and sensitivity were heavily limited by thermal background noise. With readily achievable improvements in transmitter and receiver optics, detection electronics, and filtering, it should be possible to achieve ranges of one to two kilometers at QCL power levels that seem likely in the near future. At longer ranges, however, laser speckle effects are expected to be more of a factor than they were in the initial experiments. Many improvements to the FM lidar have been made since the initial experiments, and further improvements are in progress. A second round of experiments is planned for 2003.

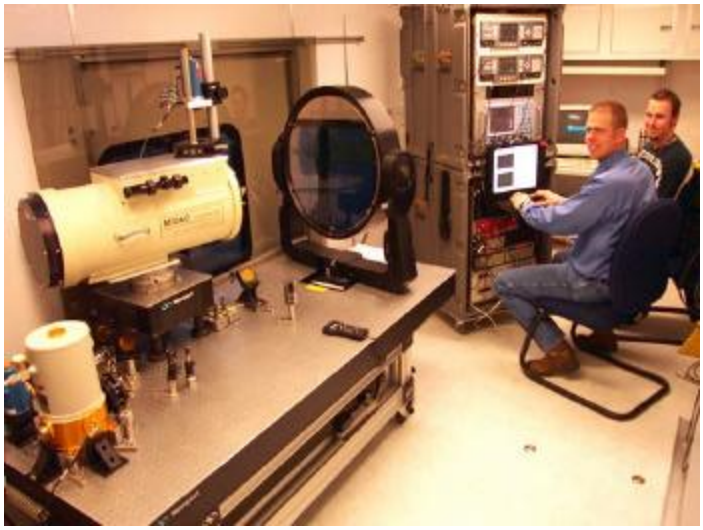

Figure 2.1: Photographs of PNNL's FM DIAL system in cart and trailer mounted configurations.

Table 2.1: Key specifications of PNNL's FM DIAL system

Configuration	Mobile cart
Receiver telescope diameter	25.4 cm (10”)
Receiver telescope focal length	76.2 cm (30”)
Detector diameter	1 mm
Detector/preamp noise floor	2.4 pA/(Hz)$^{1/2}$
Thermal background noise	3.0 pA/(Hz)$^{1/2}$
Receiver field of view (FOV)	1.3 mrad
Detection bandwidth	0.05 - 25 kHz
QC laser power	≤100 mW
QC laser wavelength	8.2 µm
QC laser divergence	1.6 mrad
Typical QC laser modulation frequency	200 kHz
Typical QC laser optical scan range	1.5 cm^{-1}
Typical QC laser modulation index	≤0.2 cm^{-1}

The preliminary bistatic and closed-loop perimeter experiments were conducted to gain experience with these configurations, and gain insight into some of the first order science and engineering considerations. As expected, the signal levels obtained at every distance were much higher than monostatic signals. The bistatic experiments were conducted along horizontal paths close to the ground in very hot weather at round-trip ranges from 0.2 to 5 kilometers, using retro-reflectors of approximately 5 and 15 cm in diameter. At round-trip ranges greater than 2 km, the return signals showed signal power fluctuations that exceed numerical predictions. For the bistatic and closed loop experiments, turbulence-driven intensity fluctuations were the limiting source of noise.

While analyzing data from the preliminary experiments, PNNL conceived and implemented two novel analysis techniques for FM DIAL data[8]. Modulating the current of any diode laser or QCL produces frequency and amplitude modulation, but for QCLs, the phase lag between the AM and FM can be quite large. For the QCL used in our experiments, the FM component of the modulation lags the AM component by 45° at modulation frequencies of 200 kHz. When a two-channel lock-in amplifier is used in the receiver, its phase can be adjusted to match that of the FM signal, so that both the full FM and part of the AM are detected on one channel, and the orthogonal signal collected *simultaneously* on the other channel consists only of the AM signal. Because both of these signals are proportional to the returned power, dividing the FM optimized signal by the orthogonal signal accomplishes normalization of the returned power. In the laboratory, this technique has been used to reduce the effects of turbulence-induced noise. As discussed in Harper et al.[7, 8], AM can also be used to quantify the burden (number density **N** times path-length through the sample **z**) of analyte present in an interrogated air sample, which cannot be done using the FM signal by itself.

2.2 Novel cavity-enhanced sensors

In 1998 researchers at the Joint Institute for Laboratory Astrophysics (JILA) reported noise-equivalent absorption sensitivity of 1×10^{-14} $cm^{-1}Hz^{-1/2}$ using a new cavity-enhanced sensing technique they named Noise-Immune, Cavity-Enhanced, Optical Heterodyne Molecular Spectroscopy (NICE-OHMS)[9]. The units used here are absorption of laser light ($\Delta I/I$) per cm of optical cavity length, per root Hertz of measurement bandwidth, or, per second of averaging time. This exceeds previous records for cavity-enhanced absorption measurements by a factor of 1000.

The extreme sensitivity demonstrated with NICE-OHMS is of interest to a wide variety of national security and civil applications because it offers potential for detecting a wide variety of important compounds that are difficult to detect with other means due to low vapor pressures. Key examples are molecular vapors associated with explosives, nerve agents, and processes for producing weapons of mass destruction. For many applications, it is highly desirable to implement NICE-OHMS in the LWIR to take advantage of distinctive molecular absorption features and atmospheric window in this region. The performance of lasers, detectors, and optics are poorer in the LWIR than at the 1.06 micron wavelength used by the JILA researchers, so LWIR performance will be poorer than the JILA results. However, LWIR NICE-OHMS holds potential for major breakthroughs in sensing capabilities if the performance of practical systems approximates the performance suggested by simple scaling calculations.

PNNL is therefore using QC lasers to explore a wide variety of CES techniques in the LWIR[2]. During the past year we stabilized QCLs to several optical cavities[10], and conducted numerous exploratory direct absorption, FM, and NICE-OHMS sensing experiments. We plan to choose the most promising techniques for the applications of interest, quantify their potential for sensitivity and selectivity, and begin exploring their performance in practical field environments.

2.2.1 Cavity-enhanced sensors with cavity-locked QCLs

A diagram of the cavity locking and absorption sensing apparatus is shown in Figure 2.2[2]. A QCL is coupled into an optical cavity via an acousto-optic modulator (AOM), and a Faraday isolator is used to prevent optical feedback into the QCL from reflecting surfaces. Reflected and transmitted signals from the optical cavity are monitored by detectors D1 and D2, respectively. The reflected cavity signals are used to lock the QCL to the peak of a TEM_{00} cavity mode using Pound-Drever-Hall (PDH) stabilization[11]. The optical cavity also forms a chamber allowing a gas sample to be exposed to the intra-cavity field at an optimal pressure. The frequency of the mode, and hence the laser, is scanned over absorption features of the analyte by supplying an appropriate sweep signal to a piezo element mounted on one of the optical cavity mirrors.

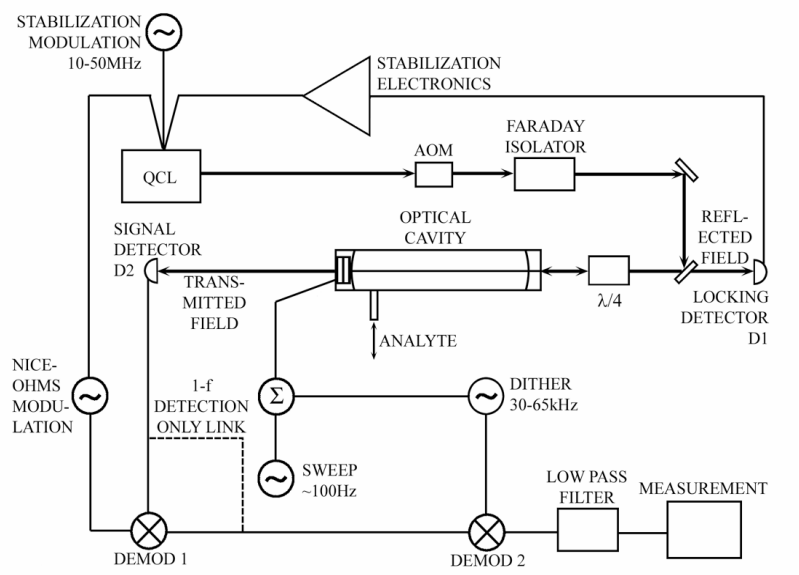

Figure 2.2: QCL-based cavity-enhanced chemical sensor, showing the QCL, isolation optics (AOM and Faraday isolator), optical cavity, reflection and transmission detectors D1 and D2. Modulation for the NICE-OHMS configuration is applied at the cavity FSR, and a secondary cavity-dither modulation is applied to a piezo element on the cavity transmission mirror. The signal due to the cavity-dither modulation alone can be monitored by using the "1-f detection only link". Similarly, the signal due to direct cavity absorption can be seen by observing the DC signal on D2 in the absence of any modulation.

Since the intensity of the mode within the cavity is extremely sensitive to optical loss, the slightest increase in absorption due to the analyte causes a dramatic reduction in cavity transmission. For very small levels of the absorption, the optical cavity represents an effective path length hundreds to thousands of times longer than its physical length, allowing a much larger detected signal, and hence improves the sensitivity of the instrument.

The increased sensitivity obtained by using an optical cavity is combined in our experiments with the techniques of frequency modulation (FM). Detecting signals at a radio frequency (RF) higher than the frequencies of technical noise in the laser and electronics, (laser power and wavelength fluctuations, and 1/f noise in the electronics), further improves signal to noise ratios. Moreover, the resonant sideband modulation technique of NICE-OHMS makes this technique immune to relative residual frequency noise between the QCL and the optical cavity. In our sensor arrangement, the NICE-OHMS modulation signal is applied directly to the QCL drive current, at a frequency equal to the free spectral range of the optical cavity, which in our case is 390 MHz for a cavity length of 38.5 cm. Sidebands and the optical carrier therefore coincide with cavity modes, allowing the intra-cavity analyte to be exposed to all components of the modulated field. Fluctuations in the amplitude or phase of the sidebands, are common-mode, and are not converted to noise as in other cavity-enhanced detection techniques.

In our experiments the optical cavity length is also dithered, causing the mode frequency to change at a rate of between 30 and 60 kHz. Since the bandwidth of the stabilization electronics is very large, the laser is forced to track these changes. This results in an additional FM process at a much lower frequency than the NICE-OHMS modulation, but with a much larger phase modulation index. Spectral features of widths corresponding to the depth of the frequency modulation are therefore selected, while narrower or broader features are rejected. These two modulation techniques are combined by first demodulating signal from the detector D2 at the NICE-OHMS frequency, and then again at the cavity-dither frequency. The result is an instrument that is immune to residual noise between the laser and the optical cavity, operates at a frequency far above that of technical noise in the laser and electronics, and can be optimized for signals of a specific spectral width. The result is an instrument that optimizes sensitivity and selectivity.

In our experimental arrangement in Figure 2.2, we can examine the response of the cavity system without modulation by monitoring the DC signals from the detector D2 directly. Alternatively, we can monitor the signal using the FM technique of cavity-dither only by bypassing the first demodulation stage of NICE-OHMS, or finally, we can observe signals using both the NICE-OHMS and cavity-dither demodulation. These three modes are discussed in detail below.

2.2.2 Cavity-enhanced sensors using direct absorption

Typical results of direct absorption experiments using the cavity-enhanced sensor are shown in Figure 2.3. For this experiment, we used cavity mirrors with reflectivities of about 99.87%, which yielded an effective path length of about

1560 meters. The traces in this figure show intensity of the cavity transmission seen at the signal detector D2 in Figure 2.2. As the sensor is scanned and absorption features are encountered, the intra-cavity absorption changes, greatly affecting the optical intensity transmitted from the cavity. The two features in the center of the scans in Figure 2.3 correspond to nitrous-oxide (N_2O) absorption lines at 1174.8283 cm^{-1} and 1174.8333 cm^{-1}, at a pressure of 180 mTorr.

These results show a scan width of up to 1.2 GHz in fully locked mode. This is currently the limit of the length change of the piezo electric actuator used to change the cavity length. If scans are taken by locking the QCL to a sequence of cavity modes, they can be pieced together to produce cavity-enhanced absorption spectra across the continuous tuning range of the QCLs, which at present is up to several cm^{-1}. The noise-limited sensitivity demonstrated in this figure is about 8.6×10^{-10} $cm^{-1}Hz^{-1/2}$. However, one of the limitations of this sensor is interference resulting from optical fringing. To the left of the N_2O features shown in Figure 2.3, there are a number of smaller peaks. These features are due to interference between reflections from the optical surfaces in the beam path - chiefly before the optical cavity. Such fringes will limit sensitivity to the extent that they have frequency characteristics similar to those of the analyte. For these results, this limit is the absorption required to produce a feature the same size as the fringing, which is about 9×10^{-7} cm^{-1}. Some of these effects may be removable with amplitude stabilization or reference subtraction techniques.

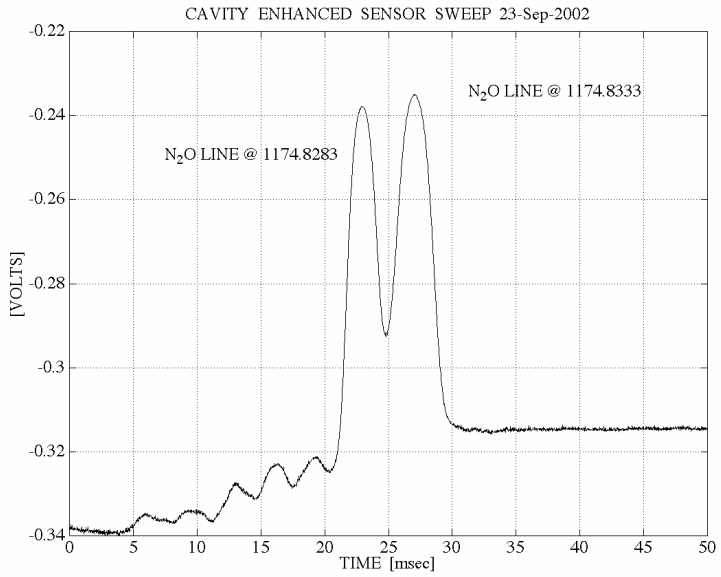

Figure 2.3: Sample output from the cavity-enhanced sensor shown in Figure 2.2 operating in direct mode; i.e., observing the DC cavity transmission directly, in the absence of modulation. Two adjacent absorption lines in pure N_2O at 180 mTorr are shown.

2.2.3 FM spectroscopy in cavity-enhanced sensors

Another way to increase the immunity of cavity-enhanced sensors to fringing and similar effects is to look for spectral features that have narrow widths and steep slopes in comparison to these effects. The homogeneous linewidth of features in the LWIR can be very narrow indeed, but are in practice limited chiefly by transit time broadening and pressure broadening to several hundred kHz. Lamb dips can be difficult to see using direct detection because they are often swamped by larger features. Since they are much narrower than the Doppler broadened profiles, however, FM spectroscopy can be employed to increase their contrast. This is because FM is most sensitive to features having spectral widths of the order of the frequency modulation depth. Using the cavity-dither modulation technique explained in the experimental description, the transmission signal seen at D2 yields dispersion-shaped features corresponding to the Lamb dips. The frequency depth of the modulation is chosen so that this process is most sensitive to features of the horizontal scale of the Lamb dips. The large Doppler-broadened features are suppressed, as is the fringing.

Typical traces from such an experiment are shown in Figure 2.4. The upper trace corresponds to 1-f detection, or simple FM spectroscopy of the Lamb dip in N_2O at 1174.901 cm^{-1}. While the 1-f Lamb dip feature is quite sharp, the gentle sloping of the trace to either side is all that remains of the Doppler-broadened line, and fringing effects of approximately the same size. Higher order detection techniques were used to take the middle and lower trances (2-f and 3-f detection, respectively), and the sloping due to the original Doppler broadened traces is no longer visible at all. These results were

taken with an early version of our optical cavity in which the mirror reflectivity was only 98.5%, and was not optimized to give extreme sensitivities. However, they illustrate the powerful selectivity of FM cavity-dither techniques very well.

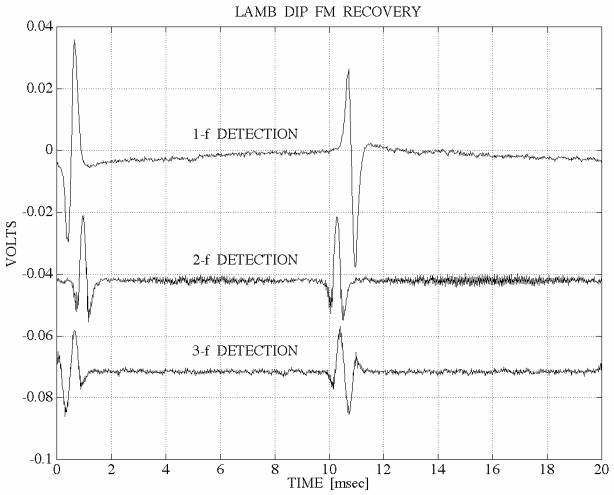

Figure 2.4: 1-f, 2-f, and 3-f detection of Lamb dips in N_2O, from top to bottom.

2.2.4 NICE-OHMS Experiments

The next step taken in our development of cavity-enhanced sensors was implementation of NICE-OHMS[2]. This technique employs both levels of modulation and recovery described in Section 2.2.1. In Figure 2.5, a comparison is made between direct cavity-enhanced detection of the Lamb dip (broadened by the cavity-dither modulation), the 1-f signal obtained using the cavity-dither method only, and the NICE-OHMS signal taken using both modulation techniques. These traces used optimum conditions, obtaining the best signal to noise ratios available at the time. In Figure 2.6, the lock between the QCL and optical cavity has been degraded to demonstrate the noise immunity of this technique. A visual inspection shows that degrading the cavity lock reduces the signal to noise ratio of the NICE-OHMS trace by a factor of 2, while the S/N ratios for 1-f recovery and direct absorption are degraded by a factor of 10, which demonstrates the noise immunity of NICE-OHMS.

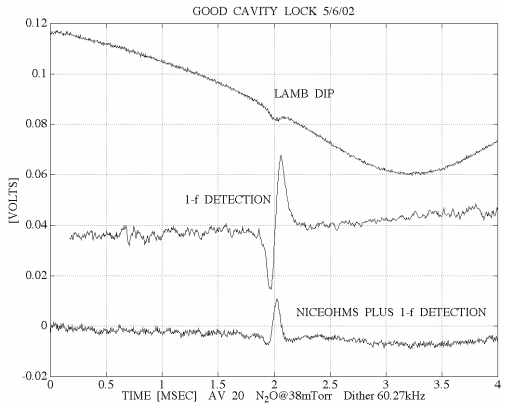

Figure 2.5: Traces showing direct absorption and the Lamb dip in direct detection (top), 1-f recovery trace (middle) and full Nice-Ohms recovery signals (bottom). The Nice-Ohms trace has a symmetric shape rather than the dispersion shape of the 1-f signal due to the extra order of demodulation.

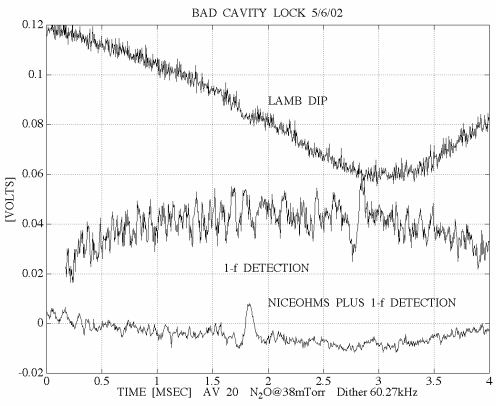

Figure 2.6: These are the same traces as shown in Figure 2.5, except that the lock between the QCL and the optical cavity was deliberately degraded. The direct absorption (top) and the 1-f recovery (middle) traces are degraded more than the Nice-Ohms trace (bottom), which is only marginally affected.

As higher mirror reflectivities are achieved in the LWIR, cavity locking will become proportionately susceptible to noise, and this advantage will become of prime importance, especially for robust, deployable sensors. With the LWIR NICE-

OHMS sensor we routinely achieve sensitivities of 8.5 x 10^{-11} cm^{-1} $Hz^{-1/2}$ using cavity mirrors with reflectivities of 99.87%. Mirrors with 99.97 % reflectivity are now available, and will be implemented during 2003.

3. QCL TRANSMITTER MODULE CONCEPTS AND RECENT RESEARCH

As shown in Figure 3.1, the general architecture for a single wavelength module of a QC transmitter for chemical sensing applications consists of a tunable, stabilized, modulated master oscillator followed by slave lasers for controlling modulation effects and amplifying optical power output. Stabilization is achieved by locking the master oscillator QCL to a Fabry-Perot cavity using Pound-Drever-Hall stabilization techniques[11]. The master oscillator is tuned by changing the length of the Fabry-Perot cavity. Known molecular absorption lines will be used to provide absolute frequency reference if required for a particular application.

The master oscillator is easily modulated at frequencies up to hundreds of megahertz by modulating its drive current, which produces both amplitude and frequency modulation. As with diode lasers, when frequency modulation (FM) is of primary interest, the amplitude modulation is called residual amplitude modulation or RAM. Pure FM is ideal for FM spectroscopy, for locking lasers to Fabry-Perot cavities for frequency stabilization, and for cavity enhanced sensors. In these applications, RAM can cause baseline shifts, harmonic distortion in the detector and its preamp, and can add baseband noise to the signal, which degrades a potentially shot noise limited measurement. As noted in Section 2.1, however, RAM is sometimes useful in FM DIAL.

The objectives for the slave and amplifier lasers shown in Figure 3.1 are to amplify master oscillator power while preserving its center wavelength, modulation, and stability characteristics. If needed for the application of interest, the slave also provides a means of suppressing RAM. This is accomplished by coupling power from the tuned, stabilized, modulated master oscillator into the slave. Because the power injected from the master is high in comparison to the power of optical noise in the slave's optical cavity, the slave follows the master's frequency rather than lasing on the frequency with maximum net gain. If the slave is operated in saturation, it will follow frequency modulation of the master, but cannot follow amplitude modulation, thus suppressing RAM. A key parameter in injection locking is the capture range, which is the maximum frequency offset between master laser and free-running slave for which the slave laser frequency will lock to injected light from the master laser. This capture range determines the required tolerance on how closely the free-running slave laser's frequency must match the master's frequency, which will determine how accurately the temperature and current of the slave laser must be controlled. The capture range also determines the master laser frequency modulation index that the slave will reproduce.

The heart of this system is the master oscillator laser, and the starting point for its development was frequency locking and stabilization[12].

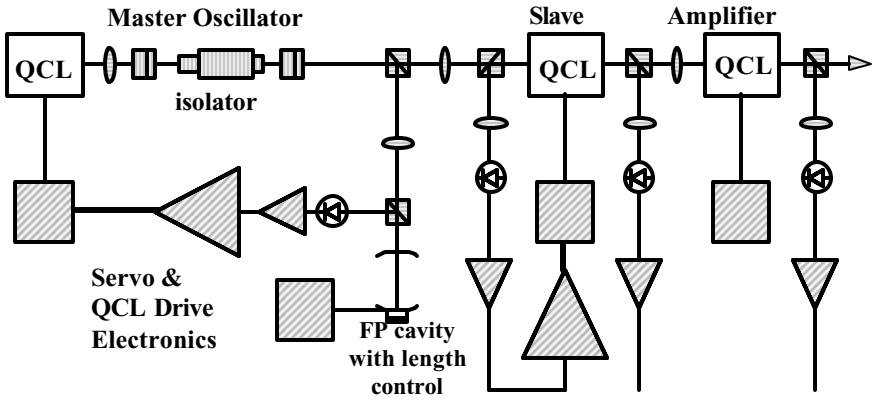

Figure 3.1: Conceptual Architecture for a Single-Wavelength QC Transmitter Module

3.1 QC laser stabilization

In November 2001 relative stabilities of approximately 5.6 Hz were achieved between two stabilized QC master oscillators operating at a wavelength of 8.5 microns[10]. This result exceeded stabilization goals by a factor of approximately 100, demonstrated that absolute stability at this level can be achieved between a QC master oscillator and a suitable absolute frequency reference, and provided the technical basis for developing the new class of ultra-sensitive chemical detection techniques described in Section 2.2. These stabilization results also provide a basis for using QCLs in precision time, frequency, or distance measurement applications, which may be of interest at some point in the future.

3.2 Frequency references

As indicated in Figure 2.1, current master oscillator concepts call for incorporation of a miniature optical cavity to provide the stable, tunable frequency reference needed for a new generation of ultra-sensitivity cavity enhanced chemical sensing techniques, and certain precision time, frequency, and distance measurement techniques. To begin miniaturizing the cavities, our goal is to reduce current cavity lengths of about 40 cm to 5 cm, and to significantly improve absolute cavity stability. A cavity frequency stability that matches the linewidth of a QCL locked to that cavity would be ideal, but a miniature cavity with a stability of a few hertz is unrealistic as such stability has only been achieved in a few fixed frequency cavities such as a single crystal sapphire cavity maintained at liquid helium temperatures. A design goal of 10 kHz frequency stability for times between 1 minute and 1 day was chosen, which is good enough to enable many high-resolution applications such as sensors based on Lamb-dips in molecular absorption lines. This stability requires the optical length of the cavity to be constant to 0.3 parts-per-billion for 10 micron lasers. For maximum utility, a reference cavity must be tunable over at least a free spectral range to allow continuous laser-frequency tuning. Two cavity designs were conceived, and construction of a prototype is beginning[12].

3.3 Injection locking and amplification

The apparatus for recent injection locking and amplification experiments is shown in Figure 3.2[12]. We injected the deflected beam from the acousto-optic modulator (AOM) into the slave laser, which was a distributed feedback QCL. The AOM shifted the frequency of the first-order deflected beam by 32 MHz, but did not shift the undeflected zero order beam. We therefore measured injection locking by monitoring the heterodyne beat note between the slave, (which was injected with the frequency-shifted first order), and the undeflected zero-order beam. When injection locking occurred, a sharp feature was observed at the AOM frequency, as shown in Figure 3.3. Figure 3.4 shows a broad beat near 32 MHz when input from the master to the slave was blocked.

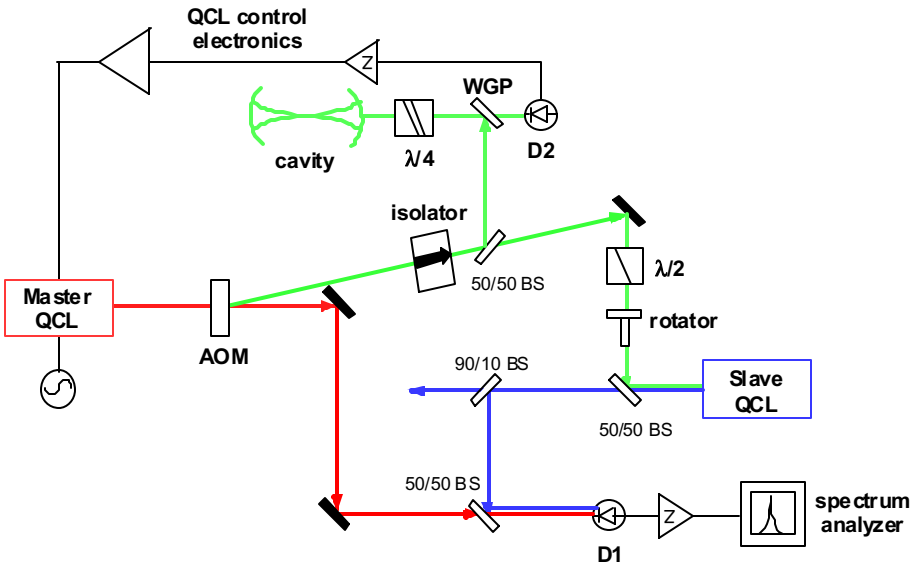

Figure 3.2: Experimental Scheme for Injection Locking

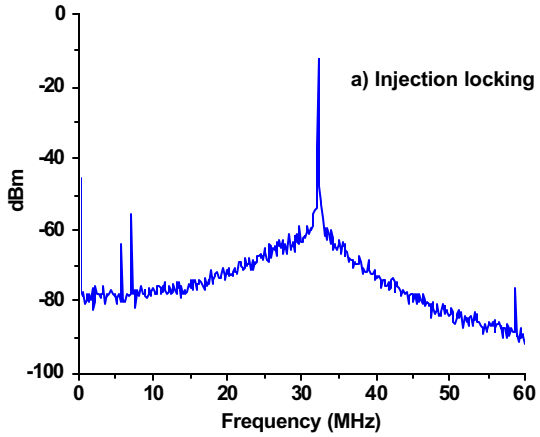

Figure 3.3: Heterodyne Beat at the AOM Frequency with Injection Locking

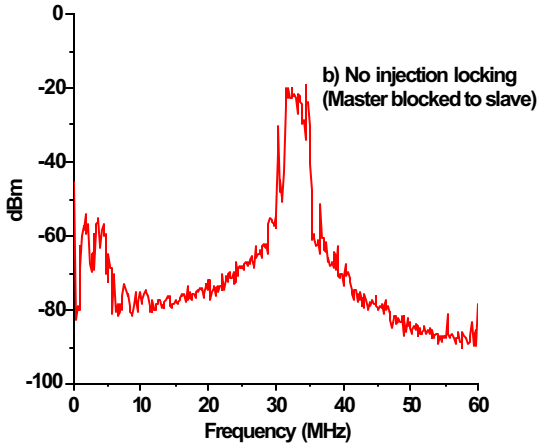

Figure 3.4: Heterodyne Beat at the AOM Frequency without Injection Locking

We also measured the injection locking range as a function of the injected power[11]. The locking range increased linearly with the square root of the injected power. With maximum injected power of 120 microwatts, the injection locking range in terms of its half-width was measured to be 500 MHz. This locking range can be improved by increasing the amount of injected power, as well as by using a Fabry-Perot slave laser.

To date, up to 49 dB of amplitude modulation suppression has been achieved in our injection locking experiments. The master laser was frequency stabilized to an optical cavity and modulated at 50 MHz, so that the master beam is characterized by the carrier frequency ω_c with two sidebands of ideally equal amplitude shifted at frequencies $\omega_c \pm 50$ MHz. Since the upper and lower sidebands are 180° out of phase, homodyne detection at the modulation frequency should yield no signal because the beat signals between the carrier and the two sidebands cancel. Amplitude modulation causes the sideband intensities to differ, and results in imperfect cancellation. We observed the signal at detector D1 from Figure 3.2 using a spectrum analyzer centered around 50 MHz. The powers on the detector were adjusted to be equivalent for both the master and the injection-locked slave beams. Figure 3.5 shows amplitude modulation at 50 MHz in which the larger signal corresponds to the amplitude modulation if only the master beam is present on the detector (i.e. the slave laser beam is blocked). This AM is quite significant and peaks at –45 dBm. Next we blocked the master and observe the AM at 50 MHz for the injection-locked slave beam, which is the smaller signal shown in Figure 3.5. The AM decreased to –94 dBm with injection locking; thus 49 dB of RAM suppression was observed. We plan to continue this experiment to quantify the effects amplitude modulation frequency and depth on AM suppression.

Given the difficulty of measuring or calculating how much power from the master oscillator is coupled through the DFB structure of the slave laser, it is difficult to quantify the degree of amplification achieved in the experiments described above. However, approximately 100 microwatts of power from the master oscillator was incident on the exterior of the slave laser's DFB structure, and the injection-locked slave's power output was nearly 4 milliwatts. At a minimum, then, the slave laser amplified the stabilized, modulated master oscillator by a factor of 40.

UCLA researchers Professor Ming Wu and Erwin Lau have adapted their numerical model of diode lasers to QCLs to model injection locking and amplification[12]. The model is a second-order, distributed, finite difference time domain solution to the coupled laser rate equations. It includes field phase and amplitude effects, as well as gain compression, distributed feedback laser gratings, linewidth enhancement, and QCL cascaded gain. They have modeled injection locking in Fabry-Perot and DFB QC lasers, modulation of multi-section QCLs with various DC biasing and AC modulation, and the effects of varying facet reflectivities. Injection locking in DFB and Fabry-Perot QCLs has been compared to study the effects of facet reflectivity, strength of grating coupling, linewidth enhancement factor, and amplitude and frequency modulation of the master laser on the locked slave laser output.

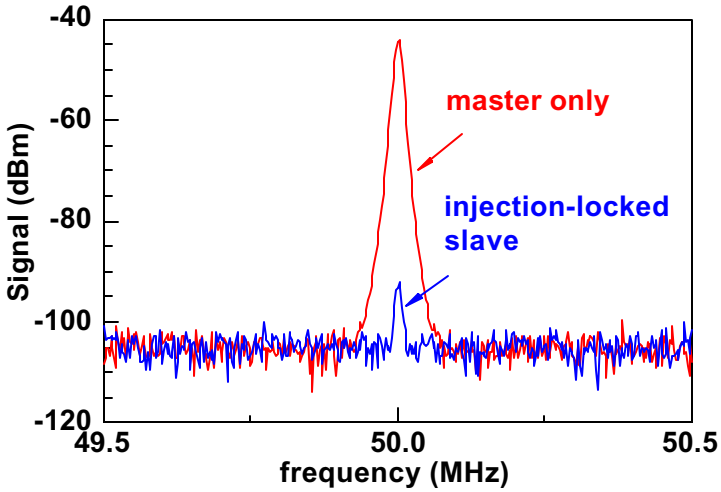

Figure 3.5: Injection Locking Suppresses Amplitude Modulation by 49 dB

The power dependence of the capture range is parameterized as the injection ratio

$$InjectionRatio = \sqrt{\frac{P_i}{P}}$$

P_i is the power incident on the slave laser facet and P is the power from the slave exiting the same facet. In the model it is assumed that the incident power is mode matched to the waveguide so that only the reflectivity of the facet reduces the amount of incident power injected into the cavity. This definition differs from the standard usage where P_i is the number of injected photons in the cavity and P is the total number of photons in the cavity, but has the advantage of being something that can be measured experimentally. In the simple lumped rate equation model of injection locking, the capture range is proportional to the injection ratio and is symmetric about the free-running slave frequency if the linewidth enhancement factor is zero. In modeling a typical DFB QCL, the capture range is proportional to the injection ratio and about 2 GHz for an injection ratio of 0.3. This capture range shows a very weak dependence on the small linewidth enhancement factors expected for QCLs. For the same QCL model, the capture range is reduced by 20% by changing from the uncoated facet reflectivities of 0.3 to facets with 99% and 1% reflectivity, which also doubles output power at the same current. Figure 3.6 shows the strength of the DFB grating has a large effect on the capture range, increasing by a factor of 3 when the grating strength is reduced to zero to model a Fabry-Perot QCL. The increased capture range of a Fabry-Perot slave also increases the maximum amplification possible when the capture range is large enough to handle a given amount of frequency modulation. This results from the amplification being the reciprocal of the square of the injection ratio. Thus, for a capture range of 2 GHz, the Fabry-Perot slave in Figure 3.6 offers an amplification of 100 compared with an amplification of 11 for the DFB slave in that figure.

In addition to predicting the capture range for injection locking QCLs, the model predicts the amplitude and frequency modulation of the locked slave laser output. For a DFB slave laser emitting 54 mW per facet and injection locked with light that has 20% RMS amplitude modulation at 100 MHz, the slave output is calculated to have 0.2% RMS amplitude modulation for a 20 dB reduction in RAM. The frequency modulation index of the injected light was 4% while that of the slave output was 3.4%. Thus for a small reduction in the FM, injection locking strongly suppressed the RAM. The model predicts that the RAM on the injection locked output can be further reduced to 0.012% RMS by a feed-forward modulation of the slave laser current similar to the work on near-IR diode lasers by Yamamoto[13].

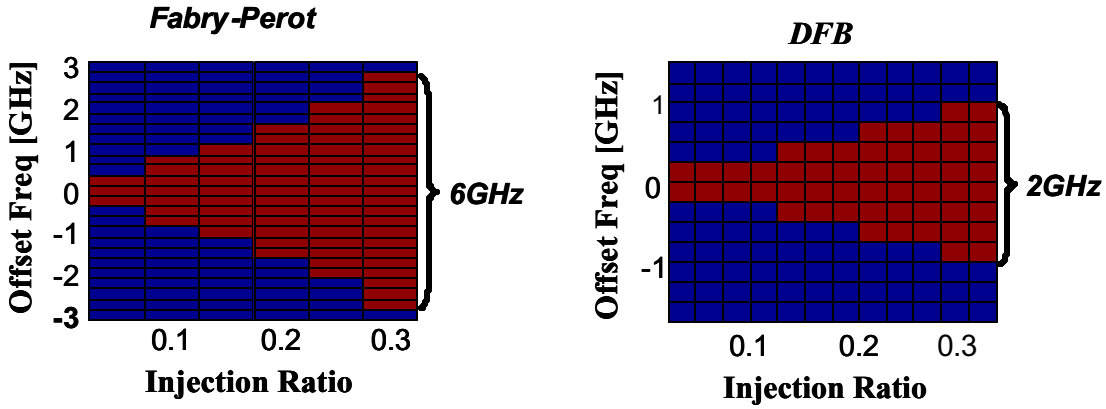

Figure 3.6: Modeling Increased Capture Range of a Fabry-Perot QCL Relative to a DFB QCL.

3.3 Quantum Cascade Lasers with Controlled End-Facet Reflectivity, and External Cavity Experiments

We envision enhancing master oscillator power output and wavelength tuning ranges through use of Fabry-Perot (FP) QC lasers placed in external optical cavities that permit control of optical output coupling, and insertion of tunable wavelength selection devices[12]. Conventional FP QCLs are formed by cleaving the ends of the laser structure to create bare facets of laser material. The reflectivities of "cavity mirrors" formed by this technique are determined by the Fresnel reflection coefficients, and are therefore fixed. While it is possible to put such a device in an external cavity, the cavity dynamics are complicated due to the presence of two sets of cavity mirrors. Full exploration and exploitation of external cavities requires FP QCLs with controlled end-facet reflectivities. Establishing control of end-facet reflectivity, however, is complicated by small end-facet dimensions, the thicknesses of optical coatings in the LWIR spectral region, and the need for QCLs to withstand thermal cycling between room temperature and cryogenic operating temperatures. Battelle recently designed and fabricated conventional coatings consisting of sputter-deposited ZnSe and Al_2O_3 layers. Unfortunately, these coatings proved unable to withstand thermal cycling.

The UCLA researchers have designed photonic band-gap reflectivity control structures that can be fabricated on the end facets of QCLs through focused ion beam milling or deep dry etching[12]. Figure 3.7 is a micrograph of a prototype milled into surrogate material. The transverse trenches in the rear form a distributed Bragg reflector (DBR). Three dimensional modeling of the waveguide, DBR structure, and light fields by the finite difference time domain (FDTD) method was used to optimize the geometry and predict a 97% reflectivity from this structure. For the anti-reflective structure on the front facet, the alternating vertical fingers and air channels form a region with an effective refractive index that matches that needed for a low reflectivity. FDTD modeling was used to optimize the geometry of this structure and predict a reflectivity of 0.4%. Ion beam milling experiments using surrogate materials were completed in July 2002. A micrograph of the results is shown in Figure 3.7. Reflectivity control structures have recently been milled into a QCL, and are being tested.

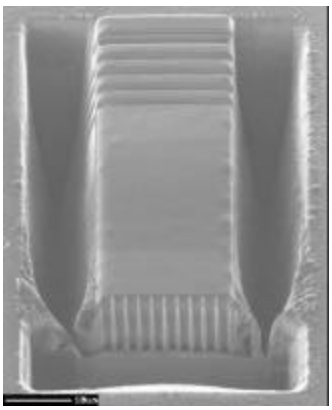

Figure 3.7: Micrograph of reflectivity control structures milled into surrogate material. The high reflectivity facet is at the top of the photograph, and the anti-reflective facet is at the bottom.

4. QUANTUM CASCADE TRANSMITTER MINIATURIZATION

Potential defense and homeland security applications such as sensors, infrared countermeasures, precision time, frequency, or distance metrology, and free-space communications will require rugged MWIR and LWIR laser transmitters with weights, volumes, and power consumption that are compatible with combat platforms, covert deployment, or sophisticated sensors for airports, cargo terminals, and other operational venues. The small physical dimensions of QCLs make it possible to envision miniaturizing QCL transmitter modules with architectures similar to the concept depicted in Figure 3.1. However, coupling laser light from one component of such a system to the other components is difficult to accomplish efficiently with free-space optics because infrared laser beams necessarily emerge from the small end-facets of QCLs with divergence angles of 60 to 70 degrees, and conventional infrared optical components such as isolators, modulators, multiplexers, and polarizers are bulky and inefficient. Currently, single-mode fibers for the MWIR and LWIR are not available. Chalcogenide glasses such as As_2Se_3 are attractive materials for MWIR and LWIR waveguide applications because they combine relatively low transmission losses with large nonlinear optical coefficients, higher thermal conductivity than other glasses, and indices of refraction between 2.4 and 2.7. In addition, they exhibit photo-modification of their indices of refraction when exposed to laser light, which opens the possibility of using lasers to write waveguides and devices in thin films of chalcogenide glasses, or in bulk structures. The large nonlinear optical coefficients of some chalcogenide glasses also hold potential for active waveguide devices such as phase modulators. Published transmission losses as low as 5.2 dB per meter[14] (for As_2Se_3 between 9.3 and 11.4 microns) indicate that integrated optical devices with path-lengths on the order of 10 centimeters or greater are feasible.

To lay the groundwork for QCL transmitter miniaturization, in 2001 PNNL started developing single-mode waveguides and waveguide-based optical components similar to those developed for short-wave infrared fiber-optic telecommunications[12]. Chalcogenide glass research is part of the development because the performance of integrated optical devices is constrained by materials chemistry, chemical compatibilities between different components, thermal effects, and optical properties of the materials, all of which are affected by materials composition and processing techniques. Relationships between chemistry, processing parameters, optical characteristics, and structural properties need to be understood to optimize the chemical composition and processing techniques, and only a small subset of the potentially useful chalcogenide glasses are commercially available. Current efforts are focused on chalcogenide glasses such as As_2S_3 and As_2Se_3, and include research on materials fabrication, laser writing, waveguide and device designs, and metrology.

4.1 Materials research

Despite relatively high bulk absorption in the MWIR and LWIR (approximately 217 dB per meter[15]), As_2S_3 was chosen as the initial material for laser writing and materials fabrication research because commercial availability of optical grade material provided a way to start the laser writing research immediately. The infrared transparency of As_2S_3 can be improved by doping with other chalcogen elements such as Se.[16] A significant body of literature on fabrication and laser writing in As_2S_3 also provided a means of measuring our progress in both areas through comparison with well-documented research. To date, commercial optical grade material used for laser-writing experiments has been examined for purity and defects, commercial bulk As_2S_3 glass has been distillation-purified, and bulk As_2S_3, As_2Se_3, and more than ten other As-S-Se glasses of varying composition have been fabricated from raw materials. Samples of materials fabricated at PNNL were successfully cut and polished, and infrared transmission been measured. Raman spectroscopy, optical microscopy, energy dispersion spectrometry (EDS) and scanning electron microscopy (SEM) are being used for additional characterization.

Commercial optical grade As_2S_3 was found to have good optical transmission, but examination with SEM and EDS revealed microscopic carbon inclusions and other imperfections on the material surface. Bulk As_2S_3 from chemical supply companies was distilled at PNNL, but was found to be too full of impurities to warrant further pursuit of this fabrication technique. During the course of distillation research, however, we discovered several different interesting microstructures with morphology that varied with surface temperature, vapor temperature, and pressure. Figure 4.1 shows some micrographs of condensed arsenic tri-sulfide structures in a region where both crystalline and amorphous deposits formed.

After the distillation experiments, many different glasses were fabricated from high purity (99.99%) starting materials, as illustrated in Figure 4.2. Infrared transmission testing was conducted with a Fourier transform infrared spectrometer (FTIR). Figure 4.3 shows that in most spectral regions, optical transmission through As_2S_3 fabricated at PNNL is essentially as good as through optical grade commercial As_2S_3, to within the limits of FTIR measurements of transmission through thin samples. As indicated in Figure 4.3, well-understood H_2O, H_2S, C, and oxide impurities resulting from inherent impurities in the source material and fabrication in uncontrolled atmospheres are thought to be responsible for the absorption bands in the PNNL material.[15-17] They will be eliminated by fabrication in controlled atmospheres.

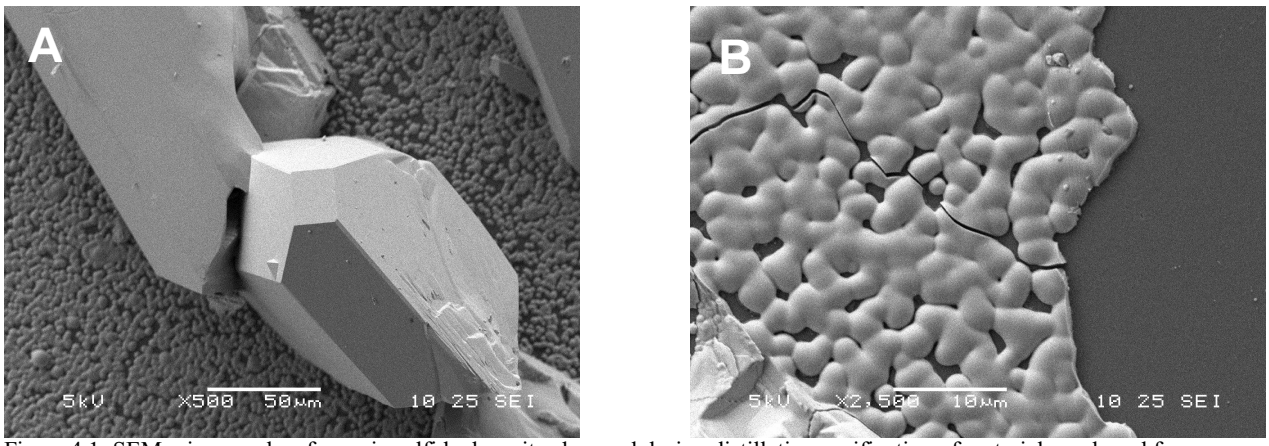

Figure 4.1: SEM micrographs of arsenic sulfide deposits observed during distillation purification of material purchased from chemical supply vendors.

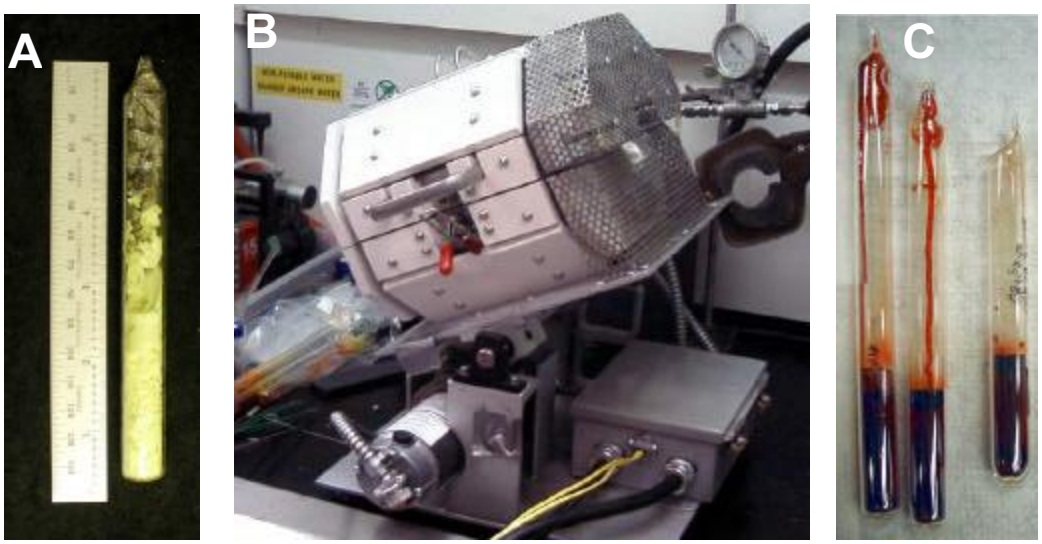

Figure 4.2: Synthesis steps for producing chalcogenide glass: (A) evacuated ampoules are made using high purity (=99.99%) elemental sources, (B) the ampoules are heated and rocked in a rocking furnace, and (C) the molten chalcogenide glass is quickly cooled to quench it into an amorphous state

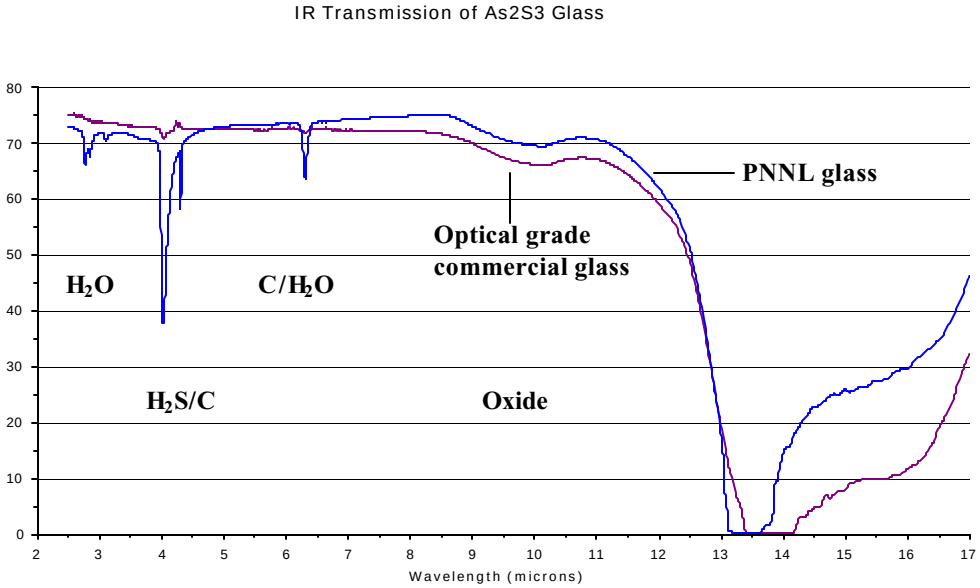

Figure 4.3: Infrared transmission of As_2S_3 glass. The transmission curves are not corrected for Fresnel reflections at the surfaces.

4.2 Laser writing

Initial waveguide writing experiments at PNNL were conducted with continuous-wave (CW) HeNe and argon-ion lasers to determine appropriate combinations of flux and fluence for writing surface structures on optical grade commercial As_2S_3. While it was frequently possible to produce waveguide-like structures, the effects of a given flux and fluence combination were inconsistent[12]. For example, a given exposure was sometimes found to result in acceptable structures at some locations on the surface, but catastrophic over-exposure at others. We think this is due to the carbon inclusions referred to in Section 4.1. As shown in Figure 4.5, sub-micron polishing imperfections in the glass surface readily mapped into laser-written structures, resulting in unacceptable non-uniformities. Under certain exposure conditions sulfur formed on the surface of laser-written As_2S_3 structures.

In July 2002 effort was shifted to writing sub-surface structures by bringing the laser light to a rapidly converging focus beneath the glass surface. Results were more consistent, and we were soon able to couple laser light through a waveguide-like linear sub-surface structure, as shown in Figure 4.6. Current effort is devoted to writing curved structures to verify that the sub-surface structures are actually guiding the light. We have also procured the equipment necessary to explore lithographic waveguide fabrication techniques.

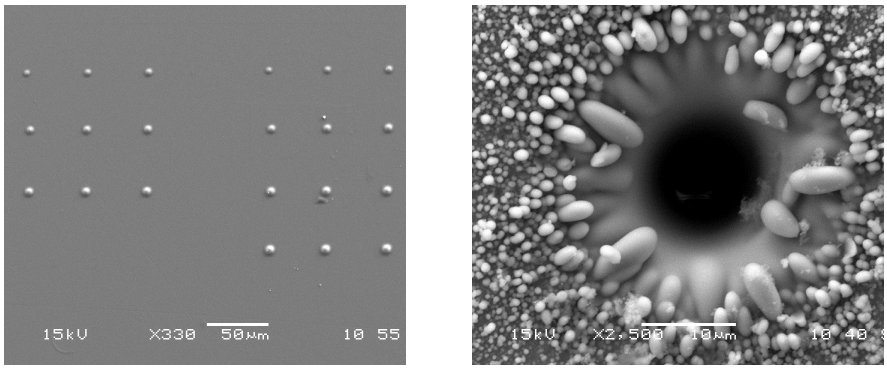

Figure 4.4: SEM micrographs of and array of spots created in As2S3 by laser-modifying the glass, and an example of the damage that can be done to chalcogenide glasses when exposed to excessive amounts of laser irradiation.

-

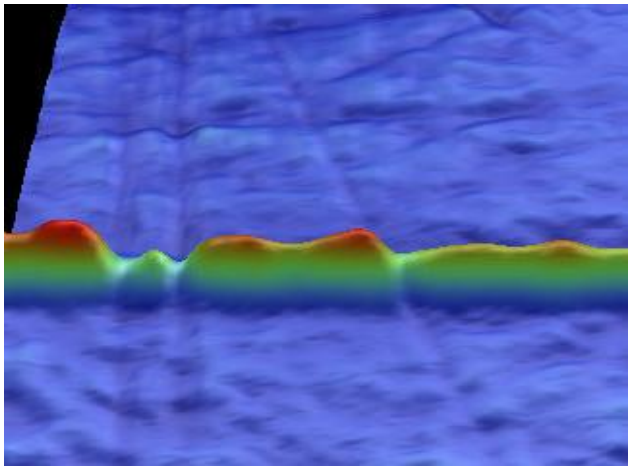

Figure 4.5: Glass surface imperfections map into laser-written linear surface structure.

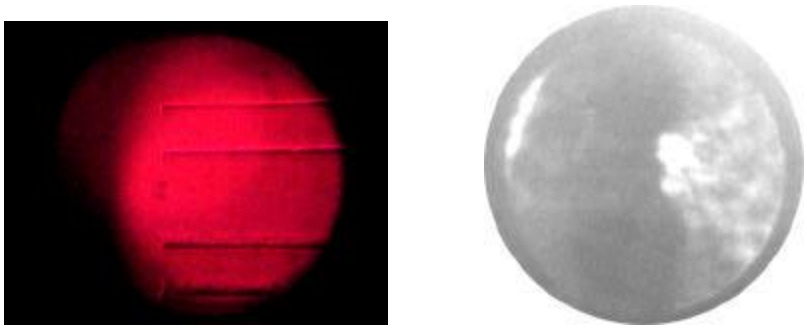

Figure 4.6: Laser-written sub-surface structures (left), and laser light coupled through one of them. The sample on the left was sliced in planes normal to the structures, and the new surfaces were optically polished. The image on the right is an end view of the structure; the bright spot is emerging laser light.

5. CONCLUSIONS

Novel techniques hold potential for tremendous improvement in the sensitivity and selectivity of spectroscopic sensing techniques, but improvements in MWIR and LWIR lasers and other laser component technology are critical to practical realization. Quantum cascade lasers are a promising laser technology due to their small size, high power, access to any wavelength between 3 and 20 microns, substantial tuning range about a chosen center wavelength, and general robustness. Good progress is being made on developing QC laser transmitters with the tunable wavelengths, frequency and amplitude stability, modulation characteristics, power levels, and wavelength multiplexing needed for new approaches to ultra-sensitive chemical detection and other applications in the infrared. Progress on QC laser transmitters is enabling demonstration of novel chemical sensing techniques. Development of materials and technology for QC transmitter miniaturization has begun.

ACKNOWLEDGEMENTS

1. The chemical sensor research was performed for the U.S. Department of Energy under Contract DE-AC06-76RL01830.
2. The laser transmitter research was performed for the U.S. Defense Advanced Research Projects Agency under Contract MDA972-01-C, and for the U.S. Department of Energy under Contract DE-AC06-76RL01830.
3. The authors are grateful to Lucent Technologies for loaning many of the lasers used in this research to PNNL.

REFERENCES

1. S.W. Sharpe et al., "Creation of 0.01 cm^{-1} Resolution, Quantitative, Infrared Spectral Libraries for Gas Samples," *Proceedings of the SPIE* #4577, pp. 12-24, 2001.
2. M.S. Taubman, R.M. Williams, T.L. Myers, and B.D. Cannon, "Ultra-Trace Chemical Sensing with Long-Wave Infrared Cavity-Enhanced Spectroscopic Sensors," *Annual Report to DOE NNSA/NA-22*, PNNL-14201 February 2003.
3. C. Gmachl, F. Capasso, D.L. Sivco, and A.Y. Cho, "Recent Progress in Quantum Cascade Laser and Applications," *Rep. Prog. Phys.* 64, pp. 1533-1601, 2001.
4. R.Q. Yang, J.L. Bradshaw, J.D. Bruno, J.T. Pham, and D.E. Wortman, "Mid-Infrared Type II Interband Cascade Lasers," *IEEE JQE* 38(6), p. 559, 2002.
5. C. Gmachl et al., "Single-Mode, Tunable Distributed-Feedback and Multiple-Wavelength Quantum Cascade Lasers," *IEEE JQE* 38(6), p. 569, 2002.
6. J.A. Silver, "Frequency-modulation spectroscopy for trace species detection: theory and comparison among experimental methods," *Applied Optics*, 31(6), pp. 707-717, 1992.
7. W.W. Harper and J.F. Schultz, "Remote Chemical Sensing Using Quantum Cascade Lasers," *Annual Report to DOE NNSA/NA-22,* PNNL-1452, December 2002.
8. W.W. Harper, D.M. Sheen, and J.F. Schultz, "FM-DIAL Preliminary Detection Sensitivity Measurements," *Special Report to DOE NNSA/NA-22*, PNNL-13992, August 2002.
9. J. Ye, L, Ma, and J.L. Hall, "Ultrasensitive detections in atomic and molecular physics: demonstration in molecular overtone spectroscopy," *J. Opt. Soc. Am B*, 15(1), pp. 6-15, 1998.
10. M.S. Taubman, T.L. Myers, B.D. Cannon, R.M. Williams, F. Capasso, C. Gmachl, D.L. Sivco, and A.Y. Cho, "Frequency stabilization of quantum-cascade lasers by use of optical cavities," *Optics Letters,* 27, pp. 2164-6, 2002.
11. R.W.P. Drever, J.L. Hall, F.V. Kowalski, J. Hough, G.M. Ford, A.J. Munley, and H. Ward, "Laser Phase and Frequency Stabilization Using an Optical Resonator," *Applied Physics B*, 31, pp. 97-105, 1983.
12. T.L. Myers, et al., "Quantum Cascade Transmitters for Advanced Military Sensors," *Semi - Annual Report to DARPA/MTO*, PNWD-3242, December 2002.
13. S. Kasapi, S. Lathi, and Y. Yamamoto, "Sub-shot-noise frequency-modulation spectroscopy by use of amplitude-squeezed light from semiconductor lasers," *J. Opt. Soc. Am. B*, 17, pp. 275-279, 2000.
14. E. Hartouni, F. Hulderman, and T. Guiton, *SPIE Proceedings* 505, pp. 131-140, 1984.
15. M.F. Churbanov et al., "Optical fibers based on As-S-Se glass system," *Journal of Non-Crystalline Solids,* 284 [1-3], pp. 146-152, 2001.
16. J.S. Savage and S. Nielsen, "Chalcogenide Glasses Transmitting In The Infrared Between 1 and 20 μ – A State of the Art Review," *Inf. Physics* 5, pp. 195-204, 1965.
17. J. Kobelke, J. Kirchhof, K. Schuster, and A. Schwuchow, "Effects of carbon, hydrocarbon and hydroxide impurities on praseodymium doped arsenic sulfide based glasses," *Journal of Non-Crystalline Solids,* 284 [1-3], pp. 123-127, 2001.